Mechanistic Insights into Specific G Protein Interactions with Adenosine Receptors

Jinan Wang, **Yinglong Miao**[*]

Center for Computational Biology and Department of Molecular Biosciences, University of Kansas, Lawrence, KS 66047, USA

Abstract

Coupling between G-protein-coupled receptors (GPCRs) and the G proteins is a key step in cellular signaling. Despite extensive experimental and computational studies, the mechanism of specific GPCR-G protein coupling remains poorly understood. This has greatly hindered effective drug design of GPCRs that are primary targets of ~1/3 of currently marketed drugs. Here, we have employed all-atom molecular simulations using a robust Gaussian accelerated molecular dynamics (GaMD) method to decipher the mechanism of the GPCR-G protein interactions. Adenosine receptors (ARs) were used as model systems based on very recently determined cryo-EM structures of the A_1AR and $A_{2A}AR$ coupled with the G_i and G_s proteins, respectively. Changing the G_i protein to the G_s led to increased fluctuations in the A_1AR and agonist adenosine (ADO), while agonist 5'-N-ethylcarboxamidoadenosine (NECA) binding in the $A_{2A}AR$ could be still stabilized upon changing the G_s protein to the G_i. Free energy calculations identified one stable low-energy conformation for each of the A_1AR-G_i and $A_{2A}AR$-G_s complexes as in the cryo-EM structures, similarly for the $A_{2A}AR$-G_i complex. In contrast, the ADO agonist and G_s protein sampled multiple conformations in the A_1AR-G_s system. GaMD simulations thus indicated that the A_1AR preferred to couple with the G_i protein to the G_s, while the $A_{2A}AR$ could couple with both the G_s and G_i proteins, being highly consistent with experimental findings of the ARs. More importantly, detailed analysis of the atomic simulations showed that the specific AR-G protein coupling resulted from remarkably complementary residue interactions at the protein interface, involving mainly the receptor transmembrane 6 helix and the G_α α5 helix and α4-β6 loop. In summary, the GaMD simulations have provided unprecedented insights into the dynamic mechanism of specific GPCR-G protein interactions at an atomistic level.

Graphical Abstract

Introduction

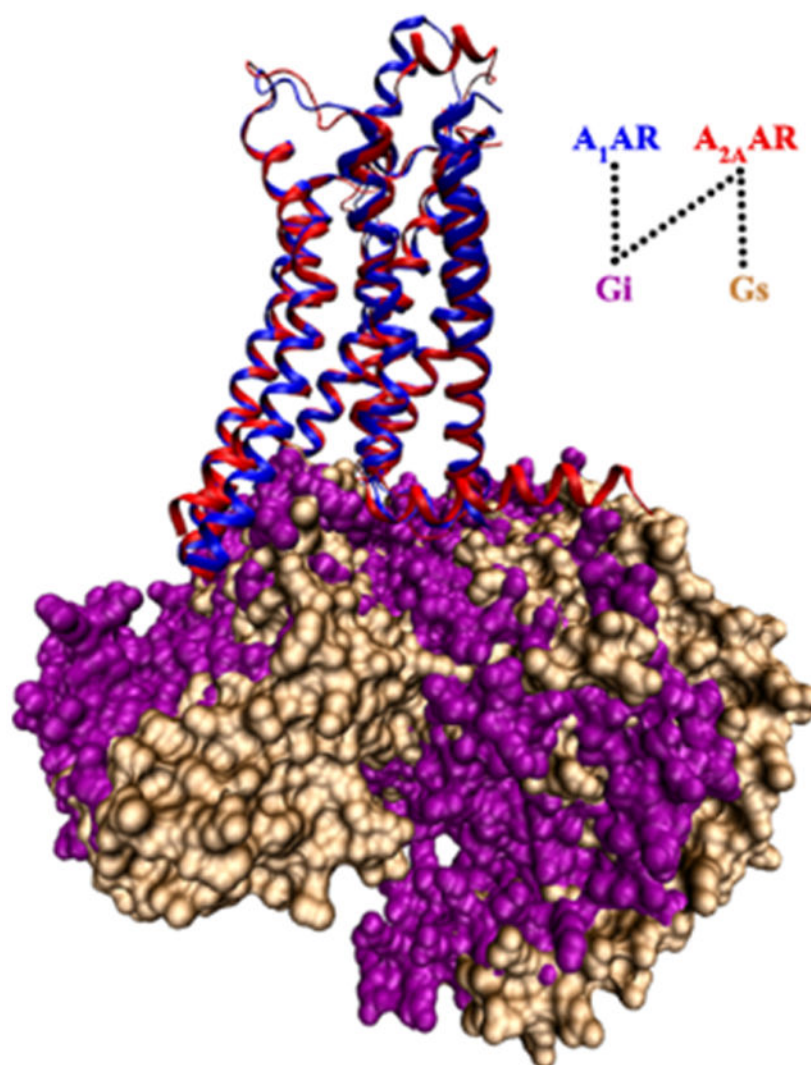G-protein-coupled receptors (GPCRs) are key cellular signaling proteins and represent
primary targets of ~1/3 of currently marketed drugs.[1] Particularly, four subtypes (A_1, A_{2A},
A_{2B}, and A_3) of GPCRs mediate the effects of adenosine, an endogenous nucleoside
modulator that plays a critical role in cytoprotective function. Adenosine receptors (ARs)
have emerged as important therapeutic targets for treating many human diseases such as
cardiac ischemia, neuropathic pain and cancer.[2] During function, the A_1AR and A_3AR
preferentially couple to the $G_{i/o}$ proteins, while the A_{2A}AR and A_{2B}AR preferentially couple
to the G_s proteins. Nevertheless, increasing evidence suggests that GPCRs including the ARs
can couple to multiple G proteins.[3-6]

Few complex structures of GPCRs coupled with the G protein or its mimic have been
determined using X-ray crystallography or cryo-EM so far.[7-11] ARs are the sole subfamily
of GPCRs that have structures in complex with different G proteins, *i.e.*, the adenosine

(ADO)-bound A_1AR coupled with the G_i protein[10] and the 5'-N-ethylcarboxamidoadenosine (NECA)-bound $A_{2A}AR$ coupled with an engineered G_s protein.[9] Both structures were obtained via cutting-edge cryo-EM and published very recently in 2018. The GPCR-G protein complex structures provide valuable information about active conformations of the GPCRs and G proteins. However, they are rather static images. The dynamic mechanism of specific GPCR–G protein interactions remains unclear.

Experimental techniques including mutagenesis, nuclear magnetic resonance, hydrogen-deuterium exchange mass spectrometry, double electron-electron resonance spectroscopy and structural biology have been utilized to investigate GPCR–G protein interactions.[12-15] While the C-terminal α_5 helix in the G_α subunit (including residues H5.22–H5.26) has been suggested as the primary driver for specific receptor recognition, the G_α α_N helix and receptor intracellular loop (ICL) 2 and transmembrane (TM) 6 helix (including residues 6.29–6.40) further contribute to the GPCR–G protein coupling specificity. The Ballesteros and Weinstein (BW) numbering[16] and common G_α numbering (CGN)[17] are used here for residues in the GPCRs and G proteins, respectively. In addition, dynamic regions in the complex and agonist binding can be crucial for the coupling through allosteric modulation.[13-14]

A bioinformatics approach has been applied to determine a selectivity barcode (patterns of amino acids) of GPCR–G protein coupling.[18] While universally conserved residues in the barcode allow GPCRs to bind and activate G protein in a similar manner, different receptors recognize the unique positions of the G-protein barcode through distinct residues. Molecular dynamics (MD) simulations have identified several important regions for coupling of the G protein with activated GPCRs, including the receptor TM6 and G_α α5 helices.[19-21] MD simulations have shown that conformational dynamics of the GPCR-G protein complex depends on the bound ligands.[22-23] Moreover, MD simulations have suggested that the binding of the active GPCR is necessary for nucleotide release from the G protein.[24-27] However, due to limited timescales, conventional MD (cMD) simulations often suffer from insufficient sampling, precluding proper free energy calculations to characterize GPCR-G protein interactions quantitatively.

To overcome the limitations of cMD, enhanced sampling methods have been applied to investigate GPCR–G protein interactions. Umbrella sampling has been used to calculate free energy profiles of the TM6 outward movement during receptor coupling to the G proteins.[21] Metadynamics simulations have been performed to investigate the dynamic effects of different GPCR ligands and intracellular binding partners[28] and examine differences of GPCRs coupled by the G protein versus its mimetic nanobody.[29] Nevertheless, these enhanced simulation methods require predefined collective variables and may apply constrains on the conformational space of the proteins. In this regard, a robust Gaussian accelerated MD (GaMD) method has been developed to allow for unconstrained enhanced sampling and free energy calculations of large biomolecules.[30-32] GaMD has been applied to successfully simulate protein folding,[30-31] protein-ligand binding and unbinding,[30-31, 33] GPCR activation,[33] large-scale conformational transitions of the CRISPR-Cas9 gene-editing system,[34] T cell receptor signaling protein,[35] human dystonia related protein,[36] and so on.

Notably, GaMD has been recently applied to capture spontaneous binding of the G-protein mimetic nanobody to a muscarinic GPCR.[37]

In this study, we have employed all-atom enhanced sampling simulations using the robust GaMD method on the latest cryo-EM structures of native ADO-A_1AR-G_i and NECA-$A_{2A}AR$-G_s protein complexes, as well as "decoy" complexes generated by switching the G proteins (Table 1 and Figure S1A in Supporting Information). A total of four simulation systems thus included the ADO-A_1AR-G_i, NECA-$A_{2A}AR$-G_s, ADO-A_1AR-G_s and NECA-$A_{2A}AR$-G_i protein complexes. To focus on the receptor-G protein coupling, we drop agonist in the complex notations for simplicity thereafter. However, note that the G protein coupling specificity may depend on the bound agonist in the receptor.[4-5] A computational model was prepared for the receptor-G protein complexes in explicit lipids and solvent (Figure S1B). The GaMD simulations allowed us to characterize structural flexibility and low-energy conformations of the AR-G protein complexes, which provided important insights into the mechanism of specific GPCR–G protein interactions.

Materials and Methods

Gaussian accelerated molecular dynamics (GaMD).

GaMD enhances the conformational sampling of biomolecules by adding a harmonic boost potential to reduce the system energy barriers.[30] When the system potential $V(\vec{r})$ is lower than a reference energy E, the modified potential $V^*(\vec{r})$ of the system is calculated as:

$$V^*(\vec{r}) = V(\vec{r}) + \Delta V(\vec{r})$$

$$\Delta V(\vec{r}) = \begin{cases} \frac{1}{2} k \big(E - V(\vec{r})\big)^2, & V(\vec{r}) < E \\ 0, & V(\vec{r}) \geq E, \end{cases}$$

(1)

Where k is the harmonic force constant. The two adjustable parameters E and k are automatically determined on three enhanced sampling principles. First, for any two arbitrary potential values $v_1(\vec{r})$ and $v_2(\vec{r})$ found on the original energy surface, if $V_1(\vec{r}) < V_2(\vec{r})$, V should be a monotonic function that does not change the relative order of the biased potential values; i.e., $V_1^*(\vec{r}) < V_2^*(\vec{r})$. Second, if $V_1(\vec{r}) < V_2(\vec{r})$, the potential difference observed on the smoothened energy surface should be smaller than that of the original; i.e., $V_2^*(\vec{r}) - V_1^*(\vec{r}) < V_2(\vec{r}) - V_1(\vec{r})$. By combining the first two criteria and plugging in the formula of $V^*(\vec{r})$ and V, we obtain

$$V_{max} \leq E \leq V_{min} + \frac{1}{k},$$

(2)

Where V_{min} and V_{max} are the system minimum and maximum potential energies. To ensure that Eq. 2 is valid, k has to satisfy: k $1/(V_{max} - V_{min}$. Let us define: $k = k_0 \cdot 1/(V_{max} -$

V_{min}, then $0 < k_0 \leq 1$. Third, the standard deviation (SD) of ΔV needs to be small enough (i.e. narrow distribution) to ensure accurate reweighting using cumulant expansion to the second order: $\sigma_{\Delta V} = k(E - V_{avg})\sigma_V \leq \sigma_0$, where V_{avg} and σ_V are the average and SD of ΔV with σ_0 as a user-specified upper limit (e.g., $10k_BT$) for accurate reweighting. When E is set to the lower bound $E = V_{max}$ according to Eq. 2, k_0 can be calculated as

$$k_0 = min(1.0, k_0') = min\left(1.0, \frac{\sigma_0}{\sigma_V} \cdot \frac{V_{max} - V_{min}}{V_{max} - V_{avg}}\right), \tag{3}$$

Alternatively, when the threshold energy E is set to its upper bound $E = V_{min} + 1/k$, k_0 is set to:

$$k_0 = k_0'' \equiv \left(1 - \frac{\sigma_0}{\sigma_V}\right) \cdot \frac{V_{max} - V_{min}}{V_{avg} - V_{min}}, \tag{4}$$

If k_0'' is calculated between 0 and 1. Otherwise, k_0 is calculated using Eq. 3.

Energetic Reweighting of GaMD Simulations.

For energetic reweighting of GaMD simulations to calculate potential of mean force (PMF), the probability distribution along a reaction coordinate is written as $p^*(A)$. Given the boost potential $\Delta V(r)$ of each frame, $p^*(A)$ can be reweighted to recover the canonical ensemble distribution $p(A)$, as:

$$p(A_j) = p^*(A_j)\frac{\langle e^{\beta\Delta V(r)}\rangle_j}{\sum_{i=1}^{M}\langle p^*(A_i)e^{\beta\Delta V(r)}\rangle_i}, \quad j = 1, ..., M, \tag{5}$$

where M is the number of bins, $\beta = k_BT$ and $\langle e^{\beta\Delta V(r)}\rangle_j$ is the ensemble-averaged Boltzmann factor of $\Delta V(r)$ for simulation frames found in the jth bin. The ensemble-averaged reweighting factor can be approximated using cumulant expansion:

$$\langle e^{\beta\Delta V(r)}\rangle = exp\left\{\sum_{k=1}^{\infty}\frac{\beta^k}{k!}C_k\right\}, \tag{6}$$

where the first two cumulants are given by:

$$C_1 = \langle \Delta V\rangle,$$
$$C_2 = \langle \Delta V^2\rangle - \langle \Delta V\rangle^2 = \sigma_v^2. \tag{7}$$

The boost potential obtained from GaMD simulations usually follows near-Gaussian distribution [32]. Cumulant expansion to the second order thus provides a good approximation for computing the reweighting factor [30, 38]. The reweighted free energy $F(A) = -k_BT \ln p(A)$ is calculated as:

$$F(A) = F^*(A) - \sum_{k=1}^{2} \frac{\beta^k}{k!} C_k + F_c, \tag{8}$$

where $F^*(A) = -k_B T \ln p^*(A)$ is the modified free energy obtained from GaMD simulation and F_c is a constant.

System Setup.

Cryo-EM structures of the A_1AR-G_i (PDB: 6D9H)[10] and $A_{2A}AR$-G_s (PDB: 6GDG)[9] were used for setting up simulation systems. Nanobody Nb35 in the cryo-EM structure of the $A_{2A}AR$-G_s was deleted for simulation. In the 6GDG cryo-EM structure, a number of residues were missing in extracellular loop (ECL) 2 and the C terminus of the $A_{2A}AR$. Because the $A_{2A}AR$ receptor configuration in the 6GDG cryo-EM structure is very similar to the X-ray structure of $A_{2A}AR$ bound by the mini-G_s protein (PDB: 5G53)[39], we added the missing residues in the ECL2 and the C terminus of the $A_{2A}AR$ using atomic coordinates from the 5G53 X-ray structure after aligning the receptor transmembrane (TM) domain of the two structures. Initial models of the A_1AR-G_s and $A_{2A}AR$-G_i protein complexes were obtained by switching the G proteins in the $A_{2A}AR$-G_s and A_1AR-G_i complexes after aligning the receptor TM domain (Figure S1A in Supporting Information). There was no steric clash between the ARs and G proteins. We calculated the number of salt-bridge, hydrogen-bonding and hydrophobic residue interactions between the receptors and G proteins at the interface in the cryo-EM (native) and computationally generated (decoy) complex structures using the LIGPLOT software.[40] As summarized in Table S1, the A_1AR-G_s decoy complex exhibited actually the largest number of residue interactions among the four systems and the $A_{2A}AR$-G_i decoy complex showed similar number of interactions as the native A_1AR-G_i complex. Therefore, all four complex structures served as good starting points for computer simulations.

According to previous findings, intracellular loop (ICL) 3 is highly flexible and removal of ICL3 does not appear to affect GPCR function.[25, 41] The ICL3 was thus omitted as in the cryo-EM structures for the simulations. [42] In addition, helical domains of the G_i and G_s proteins missing in the cryo-EM structures were not included in the simulation models.[20] This was based on earlier simulation of the β_2AR-G_s complex, which showed that the helical domain fluctuated substantially.[25] All chain termini were capped with neutral groups (acetyl and methylamide). All the disulfide bonds in the receptors and G proteins (i.e., Cys80$^{3.25}$-Cys169^{ECL2} and Cys260$^{6.61}$-Cys263^{ECL3} in the A_1AR, Cys74$^{3.22}$-Cys146^{ECL2}, Cys77$^{3.25}$-Cys166^{ECL2}, Cys71^{ECL1}-Cys159^{ECL2} and Cys259$^{6.61}$-Cys262^{ECL3} in the $A_{2A}AR$, and Cys121-Cys149 in the $G\beta$ subunit of the G_s protein) that were resolved in the cryo-EM structures were maintained in the simulations. Using the *psfgen* plugin in VMD,[43] missing atoms in protein residues were added and all protein residues were set to the standard CHARMM protonation states at neutral pH. For each of the complex systems, the receptor was inserted into a palmitoyl-oleoyl-phosphatidyl-choline (POPC) bilayer with all overlapping lipid molecules removed using the membrane plugin in VMD. The system charges were then neutralized at 0.15M NaCl using the *solvate* plugin in VMD.[43] The simulation systems were summarized in Table 1, with an example computational model shown in Supporting Information, Figure S1B.

Simulation Protocol.

The CHARMM36 parameter set[44-46] was used for the adenosine receptors, G proteins and POPC lipids. Force field parameters of agonists ADO and NECA were obtained from the CHARMM ParamChem web server.[47-48] GaMD simulations of the AR-G protein systems followed a similar protocol used in previous studies of GPCRs.[33, 37] For each of the AR-G protein complex systems, initial energy minimization, thermalization, and 20ns cMD equilibration were performed using NAMD2.12.[49] A cutoff distance of 12 Å was used for the van der Waals and short-range electrostatic interactions and the long-range electrostatic interactions were computed with the particle-mesh Ewald summation method.[50] A 2-fs integration time step was used for all MD simulations and a multiple-time-stepping algorithm was used with bonded and short-range non-bonded interactions computed every time step and long-range electrostatic interactions every two time steps. The SHAKE algorithm[51] was applied to all hydrogen-containing bonds. The NAMD simulation started with equilibration of the lipid tails. With all other atoms fixed, the lipid tails were energy minimized for 1,000 steps using the conjugate gradient algorithm and melted with a constant number, volume, and temperature (NVT) run for 0.5 ns at 310 K. The four systems were further equilibrated using a constant number, pressure, and temperature (NPT) run at 1 atm and 310 K for 10 ns with 5 kcal/(mol· Å^2) harmonic position restraints applied to the protein and ligand atoms. The system volume was found to decrease with a flexible unit cell applied and level off with 10-ns NPT run, suggesting that solvent and lipid molecules in the system were well equilibrated. Final equilibration of each system was performed using a NPT run at 1 atm pressure and 310 K for 0.5 ns with all atoms unrestrained. After energy minimization and system equilibration, conventional MD simulations were performed on each system for 20 ns at 1 atm pressure and 310 K with a constant ratio constraint applied on the lipid bilayer in the X-Y plane.

With the NAMD output structure, along with the system topology and CHARMM36 force field files, the *ParmEd* tool in the AMBER package was used to convert the simulation files into the AMBER format.[52] The GaMD module implemented in the GPU version of AMBER18[30, 52] was then applied to perform the GaMD simulation, which included a 8-ns short cMD simulation used to collect the potential statistics for calculating GaMD acceleration parameters, a 64-ns equilibration after adding the boost potential, and finally three independent 300-ns GaMD production simulations with randomized initial atomic velocities. All GaMD simulations were run at the "dual-boost" level by setting the reference energy to the lower bound. One boost potential is applied to the dihedral energetic term and the other to the total potential energetic term. The average and SD of the system potential energies were calculated every 800,000 steps (1.6 ns) for all simulation systems. The upper limit of the boost potential SD, σ_0 was set to 6.0 kcal/mol for both the dihedral and the total potential energetic terms. Similar temperature and pressure parameters were used as in the NAMD simulations. A list of GaMD production simulations on the different ARs-G proteins complex systems is listed in Table 1.

Simulation Analysis.

CPPTRAJ[53] and VMD[43] were used to analyze the GaMD simulations. Important reaction coordinates were identified from the simulation trajectories such that they involved system

dynamic regions and could be used to differentiate conformational states of the receptor-G protein complexes. The observed dynamic regions included the agonists, the receptor TM6 helix and ECL2, and the C terminus of the $G\alpha$ $\alpha5$ helix. Therefore, the root-mean square deviations (RMSDs) of the agonist and ECL2 relative to the simulation starting structures and the distance between the receptor TM3 and TM6 intracellular ends were selected as reaction coordinates. Moreover, the distance between the conserved NPxxY motif in the TM7 intracellular end of the receptors and the C terminus of the $G\alpha$ $\alpha5$ helix was used to characterize the AR-G protein interactions. Particularly, distances were calculated between the $C\alpha$ atoms of residues $Arg^{3.50}$ and $Glu^{6.30}$, the center-of-mass (COM) distance between the receptor NPxxY motif and the last 5 residues of the G_α $\alpha5$ helix, and the COM distance between the G_α (excluding residues in the αN helix) and G_β (excluding residues 2-45 in the N-terminus) subunits. Root-mean-square fluctuations (RMSFs) were calculated for the protein residues and ligands, averaged over three independent GaMD simulations and color coded for schematic representation of each complex system (Figure 1). Time courses of these reaction coordinates obtained from the GaMD simulation were plotted in Supporting Information, Figures S2-S5. The representative low-energy conformations of the AR-G protein complexes were used to compute their residue contact network at the protein interface. The residue contact network between the AR and G protein was computed using van der Waals contacts between the residue atoms. A pair of residues are in contact if the Euclidean distance between any pair of heavy atoms from the two residues is within the van der Waals interaction distance (that is, the sum of the van der Waals radii of the atoms plus 0.6 Å), as described in Reference.[54] For two-dimensional visualization, software Cytoscape[55] was utilized to plot the residue contact network.

The PyReweighting[38] toolkit was applied to reweight GaMD simulations to recover the original free energy or potential of mean force (PMF) profiles of the four AR-G protein complex systems. PMF profiles were computed using the combined trajectories from all the three independent 300 ns GaMD simulations for each system. A bin size of 1.0 Å was used for the distances and RMSDs, and 5° for the G_α $\alpha5$ orientation angle. The cutoff was set to 500 frames for 2D PMF calculations. The 2D PMF profiles were obtained for each simulation system regarding agonist RMSD relative to the cryo-EM conformation and the AR:NPxxY-G:$\alpha5$ distance (Figure 2), RMSD of the helix region in ECL2 relative to the cryo-EM structure and the AR:NPxxY-G:$\alpha5$ distance (Figures 4A and S6 in Supporting Information), the distance between atom NE1 of $Trp156^{ECL2}$ and atom O of $Gly163^{ECL2}$ and RMSD of the helix region in ECL2 relative to the cryo-EM structure (Figure S7 in Supporting Information), the $Arg^{3.50}$-$Glu^{6.30}$ and the AR:NPxxY-G:$\alpha5$ distances (Figures 4B and S8 in Supporting Information), the G_α $\alpha5$ orientation angle and the $Arg^{3.50}$-$Glu^{6.30}$ distance (Figures 4C and S9 in Supporting Information), and increase of the G_α-G_β distance and the $Arg^{3.50}$-$Glu^{6.30}$ distance (Figures 4D and S10 in Supporting Information).

Results

Variations of structural flexibility in different adenosine receptor-G protein complexes.

We first analyzed structural flexibility of both the adenosine receptors and G proteins in their complexes. In GaMD simulations of the A_1AR-G_i and $A_{2A}AR$-G_s complexes, the receptors

underwent small fluctuations except the extracellular loop 2 (ECL2) and TM6 intracellular end (Figure S11 in Supporting Information). Overall, the G proteins exhibited higher flexibility than the receptors, especially in the α5 helix, α4-β6 loop and α4-β5 loop in the G_α subunit and terminal arms of the $G_{\beta\gamma}$ subunits on the protein surface. Both the A_1AR and $A_{2A}AR$ showed flexibility change upon switching of the G proteins. For the A_1AR, changing the G_i protein to the G_s led to increased fluctuations in the ADO agonist and the receptor ECL2, TM6 intracellular end and helix 8 (H8) (Figure 1A). These motifs were suggested to be important in previous studies for activation of the A_1AR and receptor coupling with the G protein.[10, 56] For the $A_{2A}AR$, changing the G_s protein to the G_i, however, appeared to also stabilize the receptor with similar fluctuations in the latter, other than the ECL2 and intracellular loop 2 (ICL2) regions (Figure 1B).

Next, we examined flexibility change of the G proteins upon coupling to the different receptors. In the G_s protein, the C-terminus of the G_α α5 helix exhibited higher fluctuations when the $A_{2A}AR$ was changed to the A_1AR (Figure 1C). In the G_i protein, while the G_α α5 helix became stabilized with lower fluctuations, the α4-β5 loop and switch III exhibited higher flexibility when the A_1AR was changed to the $A_{2A}AR$ (Figure 1D). These regions were shown earlier to be important in activation and receptor recognition of the G protein.[25, 57]

Distinct binding modes of the G proteins and agonists in adenosine receptors.

Free energy profiles were calculated from GaMD simulations to identify low-energy conformations and binding modes of the GPCR-G protein complexes. RMSD of the agonist relative to the cryo-EM structures and the distance between the receptor NPxxY motif in the TM7 intracellular end and the C-terminus of the G_α α5 helix were first used as the reaction coordinates. In the A_1AR-G_i and $A_{2A}AR$-G_s protein complexes, both the G proteins and agonists maintained their cryo-EM conformations (Figures 2A and 2B, Table 1). In the $A_{2A}AR$-G_i complex, the NECA agonist maintained the cryo-EM conformation as in the $A_{2A}AR$-G_s complex, but the G_i protein sampled a different state with the receptor:NPxxY-G_α α5 distance decreased to ~11.2 Å (Figure 2C). The $G_{\alpha i}$ α5 helix moved ~2 Å towards the TM7 NPxxY motif of the $A_{2A}AR$ relative to the $G_{\alpha s}$ α5 helix in the $A_{2A}AR$-G_s structure (Table 1). Nevertheless, the $A_{2A}AR$-G_i complex adopted a stable low-energy conformation in the free energy profile (Figure 2C).

In the A_1AR-G_s complex, the ADO agonist exhibited fluctuations during GaMD simulations. The simulations included 8 ns short cMD, 64 ns GaMD equilibration after adding the boost potential and then three independent 300 ns GaMD production runs. Analysis of the simulation trajectories showed that RMSD of the ADO agonist reached ~5.2 Å during GaMD equilibration and up to ~12 Å in the GaMD production runs (Figure S4 in Supporting Information). Further PMF calculations identified low-energy conformational states of the ADO agonist. ADO sampled two representative conformations, denoted "L1" and "L2", for which agonist RMSD was ~3.0 Å and ~7.5 Å, respectively (Figure 2D). The "L1" conformation of ADO was similar to the cryo-EM structure with slight sliding of the purine ring by ~2 Å at the orthosteric site (Figure 3A). In the "L2" conformation, ADO formed interactions with residues $Tyr^{1.35}$ and $Tyr^{7.36}$ in the "sub-pocket 2" of the A_1AR

described earlier (Figure S12 in Supporting Information).[42] The G_s protein sampled two low-energy conformational states, which were similar to cryo-EM conformations of the G_i protein in the A_1AR-G_i complex and the G_s protein in the $A_{2A}AR$-G_s complex and thus denoted as G_i and G_s in Figure 2D. The receptor:NPxxY-G_α:α5 distance was ~11.8 Å and ~13.5 Å in the G_i- and G_s-bound A_1AR, respectively (Figure 2D and Table 1). It is important to note that GaMD simulations of the A_1AR-G_s system were not converged compared with simulations of the other systems. In this regard, the calculated free energy profiles (especially the energy barriers) were not exactly accurate. Nevertheless, we were able to identify relatively low energy wells from the PMF profiles and then representative conformational states of the A_1AR-Gs complex system.

High flexibility and conformational changes of ECL2 in the A_1AR.

The ECL2 was suggested to be important for GPCR functions[56] and observed to be highly flexible in the GaMD simulations. Thus, we analyzed its dynamics in detail here. In the A_1AR, different conformational states of the ECL2 helix were identified from GaMD simulations, including the "open", "semi-open" and "closed" state (Figure 3B). In comparison, the ECL2 in the $A_{2A}AR$ sampled only one low-energy conformational state (Figure S6 in Supporting Information). In the A_1AR-G_i complex, the ECL2 sampled a distinct "semi-open" conformation with ~5.5 Å RMSD in the helix region compared with the "open" cryo-EM conformation (Figure S6A in Supporting Information), for which the ECL2 helix tilted towards the receptor TM bundle by ~4 Å (Figure 3B). In the A_1AR-G_s system, the receptor ECL2 sampled the "open" and "closed" states (Figure 4A). In the "closed" state, the ECL2 helix tilted towards the receptor TM bundle by ~9 Å relative to the "open" cryo-EM conformation (Figure 3B). Meanwhile, the TM2 extracellular domain could move outwards by ~10 Å (Figure S7B in Supporting Information). Such movement was also observed during binding of a covalent antagonist DU172 to the A_1AR that involved an induced fit mechanism.[42, 58] In the "open" and "closed" conformational states of ECL2 in the A_1AR, residue Trp156[ECL2] formed different hydrogen bonds with Gly163[ECL2] and Val166[ECL2], respectively (Figure S7 in Supporting Information). Therefore, these residue interactions played a critical role in conformational change of ECL2 in the A_1AR. This finding was consistent with previous mutagenesis experiments, suggesting that mutations of residues Trp156[ECL2] and Val166[ECL2] affected the allosteric modulation and activation of the A_1AR.[56, 59]

Comparatively weak coupling between the A_1AR and G_s protein.

Overall, the A_1AR-G_i, $A_{2A}AR$-G_s and $A_{2A}AR$-G_i complexes appeared to be stable during the GaMD simulations (Table 1). Each of them sampled only one low-energy conformation in the free energy profiles calculated with different reaction coordinates, including the agonist RMSD (Figures 2), RMSD of the helix region in ECL2 relative to the cryo-EM/ simulation starting structures (Figure S6 in Supporting Information), the Arg[3.50]-Glu[6.30] distance (Figure S8 in Supporting Information), the G_α α5 orientation angle (Figure S9 in Supporting Information) and increase of the G_α-G_β distance from the starting conformations (Figure S10 in Supporting Information). In comparison, coupling of the G_s protein to the A_1AR was significantly weaker. The A_1AR-G_s system deviated from the simulation starting structure, visiting multiple low-energy conformational states. In particular, the TM6

intracellular end of the A_1AR sampled two distinct low-energy states. In the first state, the $Arg^{3.50}$-$Glu^{6.30}$ distance was ~17.5 Å, which is similar to that in the active cryo-EM structure (16.3 Å), thus here we referred to as "Active" state (Figure 4B). While the $Arg^{3.50}$-$Glu^{6.30}$ distance in the second state was ~22.5 Å, which is larger than the "Active" state, thus hereafter we referred to as "Over-active" state (Figure 4B). The receptor TM6 intracellular end moved ~5 Å away from the TM bundle in the "Over-active" state compared with the "Active" state (Figures 3C and 4B). When the A_1AR visited the "Active" and "Over-active" states, the G_α $\alpha 5$ helix adopted an orientation angle of ~123° and ~130° (Figure 4C) and the distance between the G_α and G_β subunits increased by ~1.2 Å and ~3.2 Å, respectively (Figure 4D).

The above results suggested that the G_s protein could not stabilize the A_1AR. On the other hand, the $G_{\alpha s}$ and $G_{\beta s}$ subunits tended to dissociate from each other when the G_s protein coupled to the A_1AR (Figure S10D in Supporting Information). In contrast, the $G_{\alpha i}$ and $G_{\beta i}$ subunits formed closer interaction when the G_i protein coupled to the A_1AR, for which the $G_{\alpha i}$-$G_{\beta i}$ distance decreased by ~1.3 Å in the energy minimum conformation of the A_1AR-G_i complex (Figure S10A). Therefore, the A_1AR induced closer interaction of the G_α and G_β subunits in the G_i protein, but dissociation of the $G_{\alpha s}$ and $G_{\beta s}$ subunits from each other (Table 1, Figure S10A and S10D in Supporting Information). In summary, coupling of A_1AR to the G_s protein was weaker than to the G_i protein.

Mechanism of specific adenosine receptor-G protein interactions.

Sequence alignments of the ARs and G proteins (Figure S13 in Supporting Information) and detailed comparison of residue interactions at the protein interface (Figure 5) enabled us to identify the origin of specific AR-G protein interactions.[10, 39, 54] In the A_1AR-G_i and $A_{2A}AR$-G_s complexes, analysis of low-energy conformations identified from the GaMD simulations highlighted specific residue interactions (Figures 5A and 5B) that were similar to those obtained previously by comparing the A_1AR-G_i and β_2AR-G_s experimental structures.[10] The last five residues of the G_α $\alpha 5$ helix formed significantly stronger receptor interactions in the A_1AR-G_i complex than in the $A_{2A}AR$-G_s complex. Residue Asp351(GH5.22) in the G_i protein formed salt-bridge interactions with $Arg^{3.53}$ and $Lys^{8.49}$ in the A_1AR. In the G_s protein, residue Glu382 (GH5.24) formed similar salt-bridge interactions with $Arg^{7.56}$ and $Arg^{8.51}$ in the $A_{2A}AR$. However, these five residues formed closer van der Waals interactions with the TM3, TM5, TM6 and H8 of the A_1AR. Second, residues GH5.8–GH5.21 of the G_α $\alpha 5$ helix formed more interactions with the receptor ICL2 and TM5 helix in the $A_{2A}AR$-G_s complex instead than in the A_1AR-G_i complex. In addition, the $\alpha 4$-$\beta 6$ loop of the G protein formed distinct interactions with the receptor TM5 helix in the $A_{2A}AR$-G_s complex compared with the A_1AR-G_i complex. Residues His347 (Gh4s6.13) and Tyr348 (Gh4s6.20) of the G_s protein formed non-polar interactions with $Gln^{5.71}$ and $Met^{5.72}$ in the $A_{2A}AR$ (Figure 5B). In contrast, residue Asp316 (Gh4s6.9) of the G_i protein formed polar interactions with residues $Lys^{6.25}$ and $Tyr^{6.26}$ in the A_1AR (Figure 5A).

In comparison, the $A_{2A}AR$-G_i complex appeared to form more residue interactions at the protein interface (Figure 5C) than both the A_1AR-G_i and $A_{2A}AR$-G_s complexes. Notably,

the last five residues of $G_{\alpha i}$ $\alpha 5$ helix formed extensive polar and non-polar interactions with the TM3, TM6, TM7, ICL2 and H8 of the $A_{2A}AR$. Residue Phe355 (GH5.26) formed close interactions with Lys $^{6.29}$, His$^{6.32}$ and Ser$^{6.36}$ of the $A_{2A}AR$. Residues GH5.8-GH5.21 of the $G_{\alpha i}$ $\alpha 5$ helix formed additional interactions with H8 of the $A_{2A}AR$, apart from those with the receptor TM5 and ICL2 as observed in the A_1AR-G_i and $A_{2A}AR$-G_s complexes. Furthermore, the $\beta 2$-$\beta 3$ loop of the G_i protein formed new interactions with the ICL2 of the $A_{2A}AR$. Residue Asp194 (Gs2s3.2) formed a salt-bridge with Arg111^{ICL2} in the $A_{2A}AR$. These interactions greatly contributed to strong coupling of the $A_{2A}AR$ and G_i protein, which showed stable low-energy conformations in the free energy profiles (e.g., Figure 2) and small fluctuations (Figure 1).

When the G_s protein coupled to the A_1AR, residue interactions at the protein interface were decreased overall (Figure 5D). In the "Active" state, the TM6 helix of the A_1AR formed significantly fewer interactions with the G_s protein (Figure 5D) than with the G_i protein (Figure 5A). The αN-$\beta 1$, $\beta 2$ sheet and $\beta 2$-$\beta 3$ loop of the G_s protein involving residues R38 (Ghns1.2), A39 (Ghns1.3), H41 (GS1.2), D215 (Gs2s3.1) and V217 (GS3.1) formed new interactions with the TM2 helix and ICL2 of the A_1AR (Figure 5D). However, both clusters of residues in the G_{α} $\alpha 5$ helix (GH5.8-GH5.21 and GH5.22-GH5.26) greatly reduced receptor interactions in the A_1AR-G_s system compared with the A_1AR-G_i and $A_{2A}AR$-G_s complexes. Similar results were observed in the "Over-active" conformation of the A_1AR-G_s system (Figure S14 in Supporting Information). Therefore, reduced residue interactions were found at the protein interface between the A_1AR and G_s protein, leading to their weaker coupling compared with the other three AR-G protein complexes (Figure 5).

In summary, the ADO-bound A_1AR preferred to bind the G_i protein to the G_s, while the $A_{2A}AR$ could bind both the G_s and G_i proteins (Figure 6). For the A_1AR, when the G_i protein was changed to the G_s, the receptor ECL2 and TM6 intracellular end underwent higher fluctuations and sampled multiple conformational states, similarly for the agonist and G protein. The G_s protein could not stabilize ADO binding in the A_1AR, and vice versa. Coupling of the A_1AR to the G_s protein was significantly weaker than to the G_i protein. The $G_{\alpha s}$ and $G_{\beta s}$ subunits tended to dissociate from each other (Figure 6A). In contrast, both the G_s and G_i proteins could stabilize agonist NECA binding in the $A_{2A}AR$. The G_i protein became even more compact with decreased distance between the G_{α} and G_{β} subunits in the NECA-bound $A_{2A}AR$-G_i complex (Figure 6B).

Discussions

ARs are so far the only subfamily of GPCRs that have available experimental structures in complex with different G proteins, including the A_1AR-G_i and $A_{2A}AR$-G_s complexes. The AR-G protein complex structures were obtained via cutting-edge cryo-EM and published very recently in 2018. Using these cryo-EM structures together with A_1AR-G_s and $A_{2A}AR$-G_i decoy complexes, we have performed all-atom enhanced simulations using the robust GaMD technique. Our GaMD simulations are shown to be converged according to time courses of system reaction coordinates in the AR-G protein complexes (Figures S2-S5 in Supporting Information) except the A_1AR-G_s decoy complex with comparatively higher fluctuations (Figure S4 in Supporting Information). Nevertheless, the all-atom GaMD

enhanced simulations have allowed us to characterize the structural flexibility and low-energy conformations of the different AR-G protein complexes, which provide valuable insights into the mechanism of specific GPCR-G protein interactions. Further detailed analysis of the AR-G protein complex simulations has highlighted a network of remarkable complementary residue interactions at the protein interface, which are important for specific G protein coupling to the A_1AR and $A_{2A}AR$.

The ADO-bound A_1AR preferred to bind the G_i protein to the G_s. This was consistent with previous experimental studies that the A_1AR coupled to different G proteins with the following rank order of "preference": $G_i>G_s>G_q$, and the G protein coupling depends on the bound agonist in the receptor.[4-5] Particularly, the NECA-bound A_1AR was shown to preferentially couple to the G_i protein compared with the G_s protein.[4] Considering similar binding affinities of ADO and NECA in the A_1AR,[60-61] the ADO-bound A_1AR likely prefers to couple to the G_i protein as well. When the A_1AR coupled with the G_s protein, the ADO agonist exhibited high fluctuations and sampled two different binding poses ("L1" and "L2"). In the "L2" binding pose, ADO formed interactions with residues $Tyr^{1.35}$ and $Tyr^{7.36}$ in the sub-pocket 2 of the A_1AR as described earlier.[42] This was similar to the 5UIG X-ray structure of the $A_{2A}AR$,[62] in which the 8D1 antagonist interacted with the same residues of the $A_{2A}AR$ (Figure S12 in Supporting Information). While the ADO and NECA agonists which bind the A_1AR and $A_{2A}AR$ in the cryo-EM structures, respectively, were used in the GaMD simulations, earlier experimental studies suggested that the coupling of different G proteins to GPCRs depends on the receptor agonist.[63-65] For the A_1AR, Cordeaux et al.[4] showed that a series of the N^6-cyclopentyladenosine (CPA) and NECA agonist analogues have different efficacies or "strengths" at activation of the G_i, G_s and G_q proteins. Agonists with the highest efficacy such as NECA could activate all the G_i, G_s and G_q proteins. Agonists with mediate strengths such as 3'-deoxy-CPA (3'dCPA) could activate the G_i and G_s proteins. The weakest agonist such as 2'dCPA could activate only the G_i protein. The role of agonists on the selectivity of GPCR-G protein coupling will be investigated in future studies. The ECL2 of the A_1AR was highly flexible (Figures 1 and S11 in Supporting Information) and sampled "open", "semi-open" and "closed" conformations (Figure S6 in Supporting Information). Both experimental and computational studies suggested that flexibility of the ECL2 was important for activation and allosteric modulation of the A_1AR.[59, 66-67] Therefore, highly flexibility of the ECL2 contributed to activation of the A_1AR and receptor coupling to the G protein.

The $A_{2A}AR$ could couple to both the G_s and G_i proteins. This correlated with a recent experimental study that the $A_{2B}AR$ coupled with both the G_s and G_i proteins in human cells.[3] The $A_{2B}AR$ was able to activate different downstream signaling pathways via different G proteins (including the G_s and G_i) in the same cell type (e.g., HEK293 kidney and T24 bladder cancer cells) and couple to the same pathway via different G proteins in different cell types.[3] Considering high similarity of $A_{2A}AR$ and $A_{2B}AR$ (72%), especially at the G protein coupling interface (Supporting Information, Figure S13B), we assume that the $A_{2A}AR$ would also couple to both the G_s and G_i proteins.

With low-energy conformations of AR-G protein complexes obtained from the GaMD simulations, further analysis revealed that complementary residue interactions were key for

specific GPCR-G protein coupling. When coupling to different G proteins, one receptor could change its conformation and flexibility (notably in the TM6 intracellular domain), similarly for one G protein as coupled to different receptors (Figures 1 and 6). Provided highly complementary residue interactions at the interface, the $A_{2A}AR$ could strongly couple to the G_s protein in addition to the G_i. However, coupling of the A_1AR to the G_s protein became weaker than to the G_i, due to significantly reduced residue interactions (Figure 5). The complementary residue interactions were identified to involve the receptor TM6, TM5, H8 and ICL2, as well as the Gα α5 helix, α4-β6 loop and αN-β1 loop. These regions have been highlighted to be important determinants for specific GPCR-G protein coupling in extensive experimental and computational studies as reviewed earlier.[12-14, 68]

In summary, the GaMD simulations with unconstrained enhanced sampling and free energy calculations have provided important insights into the mechanism of specific G protein coupling to the A_1AR and $A_{2A}AR$. Nevertheless, effects of the missing ICL3, the engineered G_s, the binding different extracellular ligands (e.g., agonists of varied potencies and allosteric modulators) on the GPCR-G protein interactions and validation of our simulation findings through biochemical and cellular experiments (notably site-directed mutagenesis) are subject to future studies. Furthermore, challenges remain to accurately predict the thermodynamic and kinetic properties of the G protein binding to the GPCRs in order to fully understand the dynamics of GPCR-G protein interactions. It is important to characterize both the association and dissociation pathways of the G protein coupling to GPCRs. Developments in computing power and enhanced simulation methodologies will be needed to address these problems in the future.

Supplementary Material

Refer to Web version on PubMed Central for supplementary material.

Acknowledgements

References:

(1). Finan C; Gaulton A; Kruger FA; Lumbers RT; Shah T; Engmann J; Galver L; Kelley R; Karlsson A; Santos R; Overington JP; Hingorani AD; Casas JP The Druggable Genome and Support for Target Identification and Validation in Drug Development. Sci. Transl. Med 2017, 9, eaag1166. [PubMed: 28356508]

(2). Jacobson KA; Gao Z-G Adenosine Receptors as Therapeutic Targets. Nat. Rev. Drug Discovery 2006, 5, 247–264. [PubMed: 16518376]

(3). Gao Z-G; Inoue A; Jacobson KA On the G Protein-coupling Selectivity of the Native A2B Adenosine Receptor. Biochem. Pharmacol 2018, 151, 201–213. [PubMed: 29225130]

(4). Cordeaux Y; IJzerman AP; Hill SJ Coupling of the Human A1 Adenosine Receptor to different Heterotrimeric G proteins: Evidence for Agonist-specific G Protein Activation. Br. J. Pharmacol 2004, 143, 705–714. [PubMed: 15302686]

(5). Cordeaux Y; Briddon SJ; Megson AE; McDonnell J; Dickenson JM; Hill SJ Influence of Receptor Number on Functional Responses Elicited by Agonists Acting at the Human Adenosine A1 Receptor: Evidence for Signaling Pathway-Dependent Changes in Agonist Potency and Relative Intrinsic Activity. Mol. Pharmacol 2000, 58, 1075–1084. [PubMed: 11040056]

(6). Stewart GD; Valant C; Dowell SJ; Mijaljica D; Devenish RJ; Scammells PJ; Sexton PM; Christopoulos A Determination of Adenosine A1 Receptor Agonist and Antagonist Pharmacology Using Saccharomyces cerevisiae: Implications for Ligand Screening and Functional Selectivity. J. Pharmacol. Exp. Ther 2009, 331, 277–286. [PubMed: 19641164]

(7). Isberg V; Mordalski S; Munk C; Rataj K; Harpsøe K; Hauser AS; Vroling B; Bojarski AJ; Vriend G; Gloriam DE GPCRdb: an Information System for G Protein-coupled Receptors. Nucleic Acids Res. 2016, 44, D356–D364. [PubMed: 26582914]

(8). Munk C; Mutt E; Isberg V; Nikolajsen LF; Bibbe JM; Flock T; Hanson MA; Stevens RC; Deupi X; Gloriam DE An Online Resource for GPCR Structure Determination and Analysis. Nat. Methods 2019, 16, 151–162. [PubMed: 30664776]

(9). García-Nafría J; Lee Y; Bai X; Carpenter B; Tate CG Cryo-EM Structure of the Adenosine A2A Receptor Coupled to an Engineered Heterotrimeric G Protein. eLife 2018, 7, e35946. [PubMed: 29726815]

(10). Draper-Joyce CJ; Khoshouei M; Thal DM; Liang YL; Nguyen ATN; Furness SGB; Venugopal H; Baltos JA; Plitzko JM; Danev R; Baumeister W; May LT; Wootten D; Sexton PM; Glukhova A; Christopoulos A Structure of the Adenosine-bound Human Adenosine A1 Receptor-Gi Complex. Nature 2018, 558, 559–563. [PubMed: 29925945]

(11). Rasmussen SGF; DeVree BT; Zou Y; Kruse AC; Chung KY; Kobilka TS; Thian FS; Chae PS; Pardon E; Calinski D; Mathiesen JM; Shah STA; Lyons JA; Caffrey M; Gellman SH; Steyaert J; Skiniotis G; Weis WI; Sunahara RK; Kobilka BK Crystal Structure of the β2 Adrenergic Receptor–Gs Protein Complex. Nature 2011, 477, 549. [PubMed: 21772288]

(12). Moreira IS Structural Features of the G-protein/GPCR Interactions. Biochim. Biophys. Acta, Gen. Subj 2014, 1840, 16–33.

(13). Mahoney JP; Sunahara RK Mechanistic Insights into GPCR–G Protein Interactions. Curr. Opin. Struct. Biol 2016, 41, 247–254. [PubMed: 27871057]

(14). Preininger AM; Meiler J; Hamm HE Conformational Flexibility and Structural Dynamics in GPCR-Mediated G Protein Activation: A Perspective. J. Mol. Biol 2013, 425, 2288–2298. [PubMed: 23602809]

(15). Duc NM; Kim HR; Chung KY Structural Mechanism of G Protein Activation by G Protein-coupled Receptor. Eur. J. Pharmacol 2015, 763, 214–222. [PubMed: 25981300]

(16). Ballesteros JA; Weinstein H Integrated Methods for the Construction of Three-dimensional Models and Computational Probing of Structure-function Relations in G Protein-coupled Receptors In Methods in Neurosciences, Sealfon SC, Ed. Academic Press: 1995; Vol. 25, pp 366–428.

(17). Flock T; Ravarani CNJ; Sun D; Venkatakrishnan AJ; Kayikci M; Tate CG; Veprintsev DB; Babu MM Universal Allosteric Mechanism for Gα Activation by GPCRs. Nature 2015, 524, 173–179. [PubMed: 26147082]

(18). Flock T; Hauser AS; Lund N; Gloriam DE; Balaji S; Babu MM Selectivity Determinants of GPCR–G-protein Binding. Nature 2017, 545, 317–322. [PubMed: 28489817]

(19). Sgourakis NG; Garcia AE The Membrane Complex between Transducin and Dark-State Rhodopsin Exhibits Large-Amplitude Interface Dynamics on the Sub-Microsecond Timescale: Insights from All-Atom MD Simulations. J. Mol. Biol 2010, 398, 161–173. [PubMed: 20184892]

(20). Van Eps N; Altenbach C; Caro LN; Latorraca NR; Hollingsworth SA; Dror RO; Ernst OP; Hubbell WL Gi- and Gs-coupled GPCRs Show Different Modes of G-protein Binding. Proc. Natl. Acad. Sci. U.S.A 2018, 115, 2383–2388. [PubMed: 29463720]

(21). Rose AS; Elgeti M; Zachariae U; Grubmüller H; Hofmann KP; Scheerer P; Hildebrand PW Position of Transmembrane Helix 6 Determines Receptor G Protein Coupling Specificity. J. Am. Chem. Soc 2014, 136, 11244–11247. [PubMed: 25046433]

(22). Goetz A; Lanig H; Gmeiner P; Clark T Molecular Dynamics Simulations of the Effect of the G-Protein and Diffusible Ligands on the β2-Adrenergic Receptor. J. Mol. Biol 2011, 414, 611–623. [PubMed: 22037586]

(23). Bai Q; Zhang Y; Ban Y; Liu H; Yao X Computational Study on the Different Ligands Induced Conformation Change of β2 Adrenergic Receptor-Gs Protein Complex. PLoS One 2013, 8, e68138. [PubMed: 23922653]

(24). Pachov DV; Fonseca R; Arnol D; Bernauer J; van den Bedem H Coupled Motions in β2AR: Gαs Conformational Ensembles. J. Chem. Theory Comput 2016, 12, 946–956. [PubMed: 26756780]

(25). Dror RO; Mildorf TJ; Hilger D; Manglik A; Borhani DW; Arlow DH; Philippsen A; Villanueva N; Yang Z; Lerch MT Structural Basis for Nucleotide Exchange in Heterotrimeric G Proteins. Science 2015, 348, 1361–1365. [PubMed: 26089515]

(26). Louet M; Perahia D; Martinez J; Floquet N A Concerted Mechanism for Opening the GDP Binding Pocket and Release of the Nucleotide in Hetero-Trimeric G-Proteins. J. Mol. Biol 2011, 411, 298–312. [PubMed: 21663745]

(27). Louet M; Martinez J; Floquet N GDP Release Preferentially Occurs on the Phosphate Side in Heterotrimeric G-proteins. PLoS Comput. Biol 2012, 8, e1002595. [PubMed: 22829757]

(28). Saleh N; Saladino G; Gervasio FL; Clark T Investigating Allosteric Effects on the Functional Dynamics of β2-adrenergic Ternary Complexes with Enhanced-sampling Simulations. Chem. Sci 2017, 8, 4019–4026. [PubMed: 30155211]

(29). Saleh N; Ibrahim P; Clark T Differences between G-Protein-Stabilized Agonist-GPCR Complexes and their Nanobody-Stabilized Equivalents. Angew. Chem. Int. Ed. Engl 2017, 56, 9008–9012. [PubMed: 28481446]

(30). Miao Y; Feher VA; McCammon JA Gaussian Accelerated Molecular Dynamics: Unconstrained Enhanced Sampling and Free Energy Calculation. J. Chem. Theory Comput 2015, 11, 3584–3595. [PubMed: 26300708]

(31). Pang YT; Miao Y; Wang Y; McCammon JA Gaussian Accelerated Molecular Dynamics in NAMD. J. Chem. Theory Comput 2017, 13, 9–19. [PubMed: 28034310]

(32). Miao Y; McCammon JA Gaussian Accelerated Molecular Dynamics: Theory, Implementation, and Applications. Annu. Rep. Comput. Chem 2017, 13, 231–278. [PubMed: 29720925]

(33). Miao Y; McCammon JA Graded Activation and Free Energy Landscapes of a Muscarinic G-protein–coupled Receptor. Proc. Natl. Acad. Sci. U.S.A 2016, 113, 12162–12167. [PubMed: 27791003]

(34). Palermo G; Miao YL; Walker RC; Jinek M; McCammon JA CRISPR-Cas9 Conformational Activation as Elucidated from Enhanced Molecular Simulations. Proc. Natl. Acad. Sci. U.S.A 2017, 114, 7260–7265. [PubMed: 28652374]

(35). Sibener LV; Fernandes RA; Kolawole EM; Carbone CB; Liu F; McAffee D; Birnbaum ME; Yang XB; Su LF; Yu W; Dong S; Gee MH; Jude KM; Davis MM; Groves JT; Goddard WA; Heath JR; Evavold BD; Vale RD; Garcia KC Isolation of a Structural Mechanism for Uncoupling T Cell Receptor Signaling from Peptide-MHC Binding. Cell 2018, 174, 672–687.e27. [PubMed: 30053426]

(36). Salawu EO The Impairment of TorsinA's Binding to and Interactions With Its Activator: An Atomistic Molecular Dynamics Study of Primary Dystonia. Front. Mol. Biosci 2018, 5, 64. [PubMed: 30042949]

(37). Miao Y; McCammon JA Mechanism of the G-protein Mimetic Nanobody Binding to a Muscarinic G-protein-coupled Receptor. Proc. Natl. Acad. Sci. U.S.A 2018, 115, 3036–3041. [PubMed: 29507218]

(38). Miao Y; Sinko W; Pierce L; Bucher D; Walker RC; McCammon JA Improved Reweighting of Accelerated Molecular Dynamics Simulations for Free Energy Calculation. J. Chem. Theory Comput 2014, 10, 2677–2689. [PubMed: 25061441]

(39). Carpenter B; Nehmé R; Warne T; Leslie AGW; Tate CG Structure of the Adenosine A2A Receptor Bound to an Engineered G protein. Nature 2016, 536, 104–107. [PubMed: 27462812]

(40). Wallace AC; Laskowski RA; Thornton JM LIGPLOT: a Program to Generate Schematic Diagrams of Protein-ligand Interactions. Protein Eng. 1995, 8, 127–134. [PubMed: 7630882]

(41). Dror RO; Arlow DH; Maragakis P; Mildorf TJ; Pan AC; Xu H; Borhani DW; Shaw DE Activation Mechanism of the β2-adrenergic Receptor. Proc. Natl. Acad. Sci. U.S.A 2011, 108, 18684–18689. [PubMed: 22031696]

(42). Glukhova A; Thal DM; Nguyen AT; Vecchio EA; Jörg M; Scammells PJ; May LT; Sexton PM; Christopoulos A Structure of the Adenosine A1 Receptor Reveals the Basis for Subtype Selectivity. Cell 2017, 168, 867–877.e13. [PubMed: 28235198]

(43). Humphrey W; Dalke A; Schulten K VMD: Visual Molecular Dynamics. J. Mol. Graphics 1996, 14, 33–38.

(44). Vanommeslaeghe K; MacKerell AD CHARMM Additive and Polarizable Force Fields for Biophysics and Computer-aided Drug Design. Biochim. Biophys. Acta, Gen. Subj 2015, 1850, 861–871.

(45). Huang J; Rauscher S; Nawrocki G; Ran T; Feig M; de Groot BL; Grubmüller H; MacKerell AD Jr CHARMM36m: an Improved Force Field for Folded and Intrinsically Disordered Proteins. Nat. Methods 2016, 14, 71–73. [PubMed: 27819658]

(46). Klauda JB; Venable RM; Freites JA; O'Connor JW; Tobias DJ; Mondragon-Ramirez C; Vorobyov I; MacKerell AD; Pastor RW Update of the CHARMM All-Atom Additive Force Field for Lipids: Validation on Six Lipid Types. J. Phys. Chem. B 2010, 114, 7830–7843. [PubMed: 20496934]

(47). Vanommeslaeghe K; Raman EP; MacKerell AD Jr. Automation of the CHARMM General Force Field (CGenFF) II: Assignment of Bonded Parameters and Partial Atomic Charges. J. Chem. Inf. Model 2012, 52, 3155–3168. [PubMed: 23145473]

(48). Vanommeslaeghe K; MacKerell AD Jr. Automation of the CHARMM General Force Field (CGenFF) I: Bond Perception and Atom Typing. J. Chem. Inf. Model 2012, 52, 3144–3154. [PubMed: 23146088]

(49). Phillips JC; Braun R; Wang W; Gumbart J; Tajkhorshid E; Villa E; Chipot C; Skeel RD; Kale L; Schulten K Scalable Molecular Dynamics with NAMD. J. Comput. Chem 2005, 26, 1781–802. [PubMed: 16222654]

(50). Darden T; York D; Pedersen L Particle Mesh Ewald: An N· log (N) Method for Ewald Sums in Large Systems. J. Chem. Phys 1993, 98, 10089.

(51). Ryckaert J-P; Ciccotti G; Berendsen HJ Numerical Integration of the Cartesian Equations of Motion of a System with Constraints: Molecular Dynamics of N-alkanes. J. Comput. Phys 1977, 23, 327–341.

(52). Case D, et al. , Amber 18 (University of California, San Francisco). 2018.

(53). Roe DR; Cheatham TE 3rd. PTRAJ and CPPTRAJ: Software for Processing and Analysis of Molecular Dynamics Trajectory Data. J. Chem. Theory Comput 2013, 9, 3084–3095. [PubMed: 26583988]

(54). Venkatakrishnan AJ; Deupi X; Lebon G; Tate CG; Schertler GF; Babu MM Molecular Signatures of G-protein-coupled Receptors. Nature 2013, 494, 185–194. [PubMed: 23407534]

(55). Shannon P; Markiel A; Ozier O; Baliga NS; Wang JT; Ramage D; Amin N; Schwikowski B; Ideker T Cytoscape: a Software Environment for Integrated Models of Biomolecular Interaction Networks. Genome Res. 2003, 13, 2498–504. [PubMed: 14597658]

(56). Nguyen ATN; Baltos J-A; Thomas T; Nguyen TD; Muñoz LL; Gregory KJ; White PJ; Sexton PM; Christopoulos A; May LT Extracellular Loop 2 of the Adenosine A1 Receptor Has a Key Role in Orthosteric Ligand Affinity and Agonist Efficacy. Mol. Pharmacol 2016, 90, 703–714. [PubMed: 27683014]

(57). Oldham WM; Hamm HE Heterotrimeric G protein Activation by G-protein-coupled Receptors. Nat. Rev. Mol. Cell Biol 2008, 9, 60–71. [PubMed: 18043707]

(58). Cheng RKY; Segala E; Robertson N; Deflorian F; Doré AS; Errey JC; Fiez-Vandal C; Marshall FH; Cooke RM Structures of Human A1 and A2A Adenosine Receptors with Xanthines Reveal Determinants of Selectivity. Structure 2017, 25, 1275–1285. [PubMed: 28712806]

(59). Peeters MC; Wisse LE; Dinaj A; Vroling B; Vriend G; Ijzerman AP The Role of the Second and Third Extracellular Loops of the Adenosine A1 Receptor in Activation and Allosteric Modulation. Biochem. Pharmacol 2012, 84, 76–87. [PubMed: 22449615]

(60). Nair V; Fesbender AJ; Miller LP; Bruce JL High Selectivity of Novel Isoguanosine Analogues for the Adenosine A1 Receptor. Bioorg. Med. Chem. Lett 1991, 1, 481–486.

(61). de Lera Ruiz M; Lim Y-H; Zheng J Adenosine A2A Receptor as a Drug Discovery Target. J. Med. Chem 2014, 57, 3623–3650. [PubMed: 24164628]

(62). Sun B; Bachhawat P; Chu ML-H; Wood M; Ceska T; Sands ZA; Mercier J; Lebon F; Kobilka TS; Kobilka BK Crystal Structure of the Adenosine A2A Receptor Bound to an Antagonist Reveals a Potential Allosteric Pocket. Proc. Natl. Acad. Sci. U.S.A 2017, 114, 2066–2071. [PubMed: 28167788]

(63). Woo AY; Wang T; Zeng X; Zhu W; Abernethy DR; Wainer IW; Xiao R-P Stereochemistry of an Agonist Determines Coupling Preference of β2-Adrenoceptor to Different G Proteins in Cardiomyocytes. Mol. Pharmacol 2009, 75, 158–165. [PubMed: 18838481]

(64). Stallaert W; Christopoulos A; Bouvier M Ligand Functional Selectivity and Quantitative Pharmacology at G protein-coupled Receptors. Expert Opin. Drug Discovery 2011, 6, 811–825.

(65). Jockers R; Linder ME; Hohenegger M; Nanoff C; Bertin B; Strosberg AD; Marullo S; Freissmuth M Species Difference in the G Protein Selectivity of the Human and Bovine A1-adenosine Receptor. J. Biol. Chem 1994, 269, 32077–84. [PubMed: 7798201]

(66). Nguyen ATN; Vecchio EA; Thomas T; Nguyen TD; Aurelio L; Scammells PJ; White PJ; Sexton PM; Gregory KJ; May LT; Christopoulos A Role of the Second Extracellular Loop of the Adenosine A1 Receptor on Allosteric Modulator Binding, Signaling, and Cooperativity. Mol. Pharmacol 2016, 90, 715–725. [PubMed: 27683013]

(67). Miao Y; Bhattarai A; Nguyen ATN; Christopoulos A; May LT Structural Basis for Binding of Allosteric Drug Leads in the Adenosine A1 Receptor. Sci. Rep 2018, 8, 16836. [PubMed: 30442899]

(68). Wang J; Miao Y Recent Advances in Computational Studies of GPCR-G Protein Interactions. Adv. Protein Chem. Struct. Biol 2019, 116, 397–419. [PubMed: 31036298]
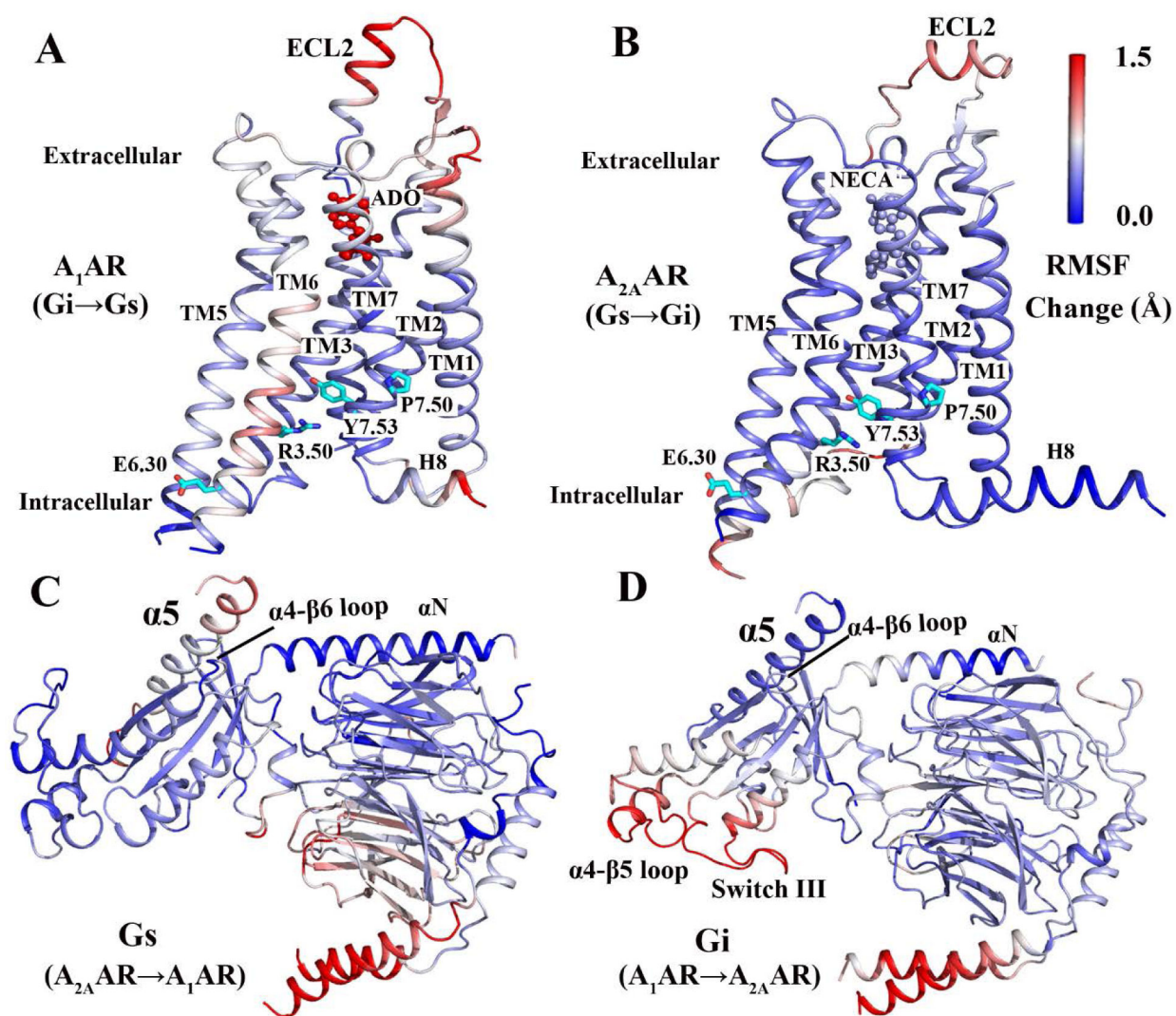
Figure 1.

Comparison of structural flexibility of active adenosine receptor-G protein complexes obtained from GaMD simulations: **(A)** Change in the root-mean-square fluctuations (RMSFs) of the A_1AR when the G_i protein was changed to the G_s protein. **(B)** Change in the RMSFs of the $A_{2A}AR$ when the G_s protein was changed to the G_i protein. **(C)** Change in the RMSFs of the G_s protein when the receptor was changed from the $A_{2A}AR$ to the A_1AR. **(D)** Change in the RMSFs of the G_i protein when the receptor was changed from the A_1AR to the $A_{2A}AR$. A color scale of 0.0 Å (blue) to 1.5 Å (red) is used.
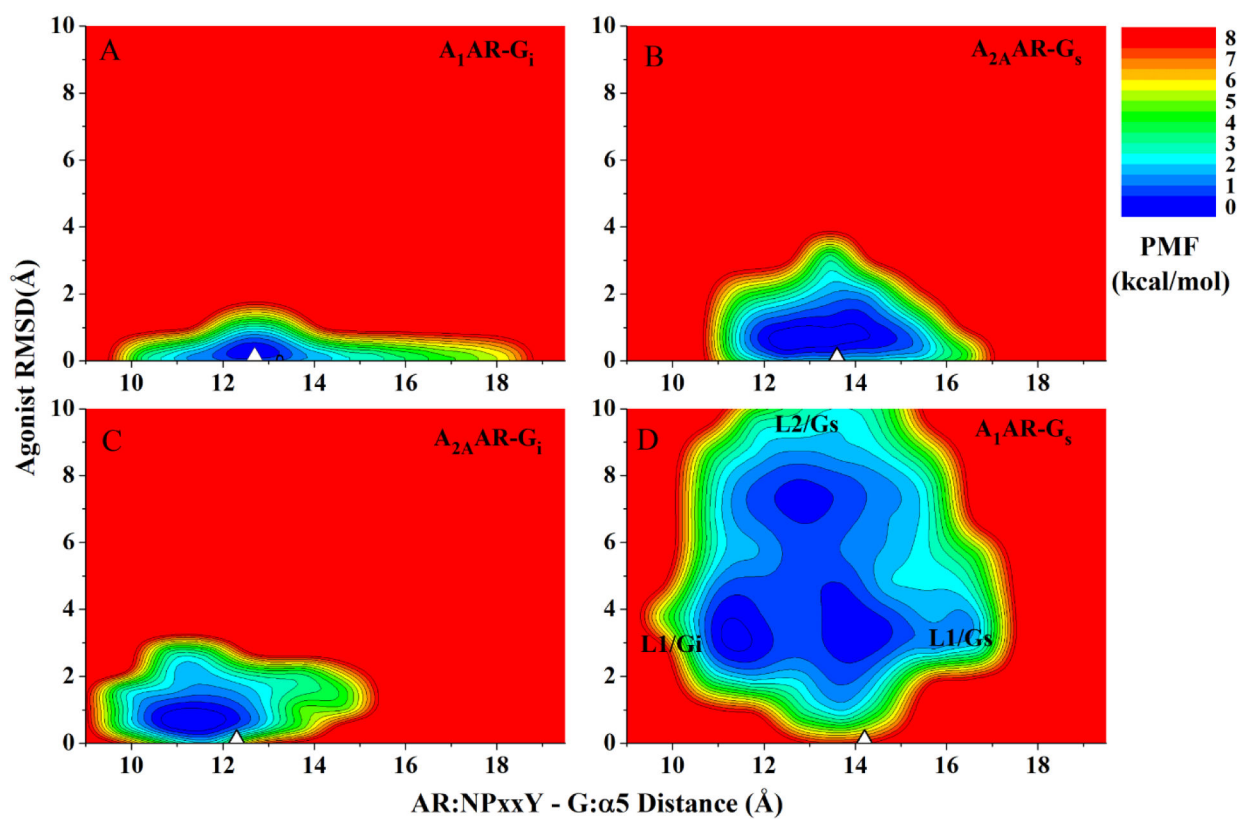
Figure 2.
2D potential of mean force (PMF) profiles of the **(A)** A_1AR-G_i, **(B)** $A_{2A}AR-G_s$, **(C)** $A_{2A}AR-G_i$ and **(D)** A_1AR-G_s complex systems regarding the agonist RMSD relative to the cryo-EM conformation and AR:NPxxY-G:α5 distance. The white triangles indicate the cryo-EM or simulation starting structures.
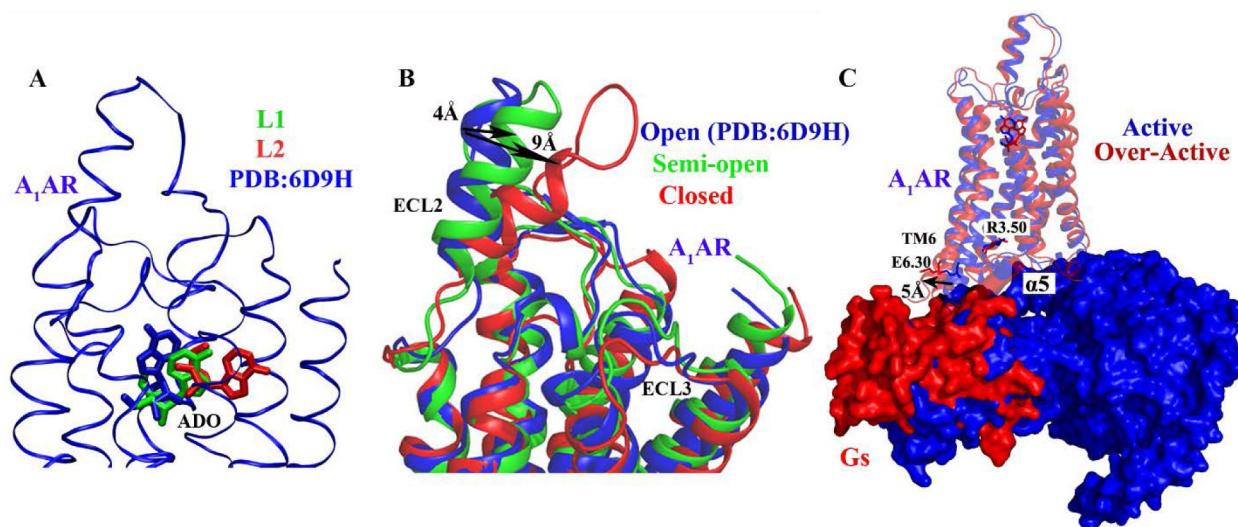
Figure 3.
Distinct active conformations of the A_1AR induced by binding of the G_s protein: **(A)** Representative conformations of two low-energy binding poses of ADO (L1 and L2 in green and red, respectively) in the A_1AR-G_s complex. The cryo-EM structure of the A_1AR-G_i complex (PDB: 6D9H, blue) is shown for comparison. **(B)** Representative conformations of open (PDB: 6D9H, blue), semi-open (green) and closed (red) states of ECL2 in the A_1AR. **(C)** Representative conformations of the A_1AR in the "Active" (blue) and "Over-active" (red) states in the A_1AR-G_s system.
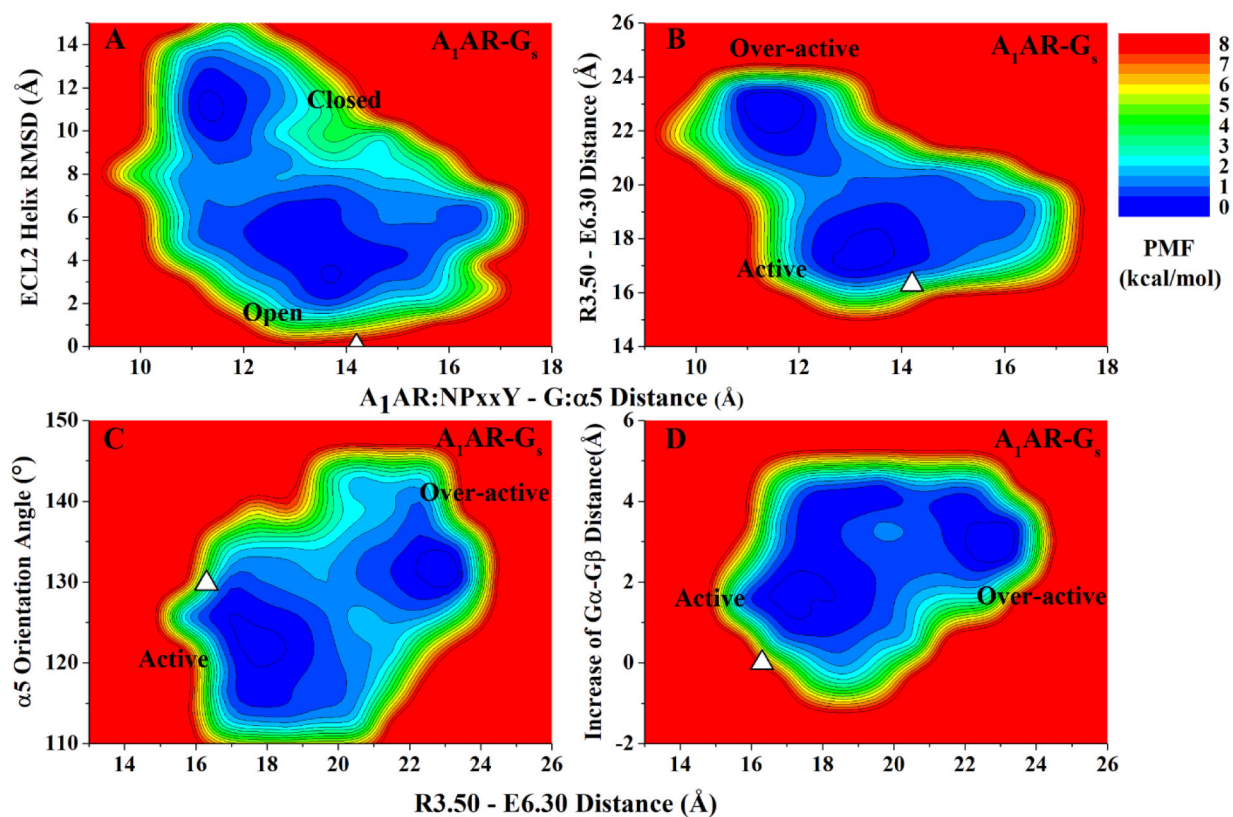
Figure 4.
Distinct low-energy conformational states of the A_1AR-G_s system were identified from GaMD simulations. **(A)** 2D PMF of RMSD of the helix region in ECL2 relative to the cryo-EM structure and the A_1AR: NPxxY-G: α5 distance. **(B)** 2D PMF of the R3.50-E6.30 and A_1AR: NPxxY-G: α5 distances. **(C)** 2D PMF of the orientation angle of the Gα α5 helix and the R3.50-E6.30 distance. **(D)** 2D PMF of the increase of the G_α-G_β distance and the R3.50-E6.30 distance. The white triangles indicate the cryo-EM or simulation starting structures.
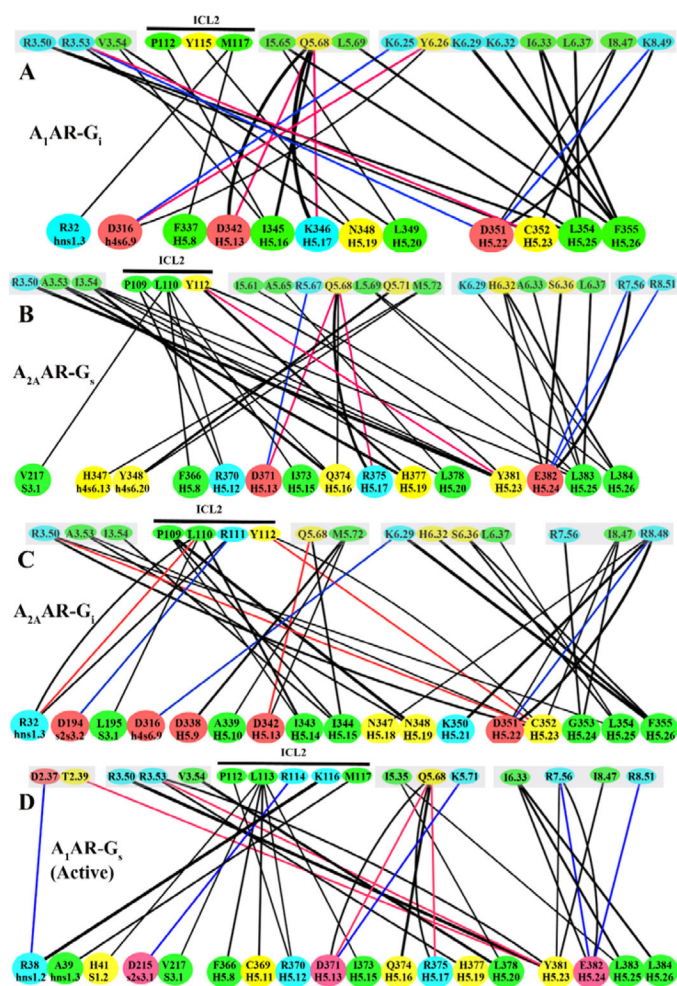
Figure 5.
Complementary residue interactions at the protein interface in the (**A**) A$_1$AR-G$_i$, (**B**) A$_{2A}$AR-G$_s$, (**C**) A$_{2A}$AR-G$_i$ and (**D**) A$_1$AR-G$_s$ (active state) systems. The representative low-energy conformations of the complexes were used to calculate these interaction contacts. Hydrogen bond, van der Waals and salt-bridge interactions are colored in red, black and blue, respectively. The line thickness is proportional to the number of residue interaction pairs. Hydrophobic, polar, acidic and basic residues are colored in green, yellow, red and blue, respectively. For receptors, the BW numbers are used for residues in the TM helices and the original index numbers for residues in the receptor loops. For the G proteins, the residue one letter code and original index number are labeled in the first row and the residue CGN number in the second row.
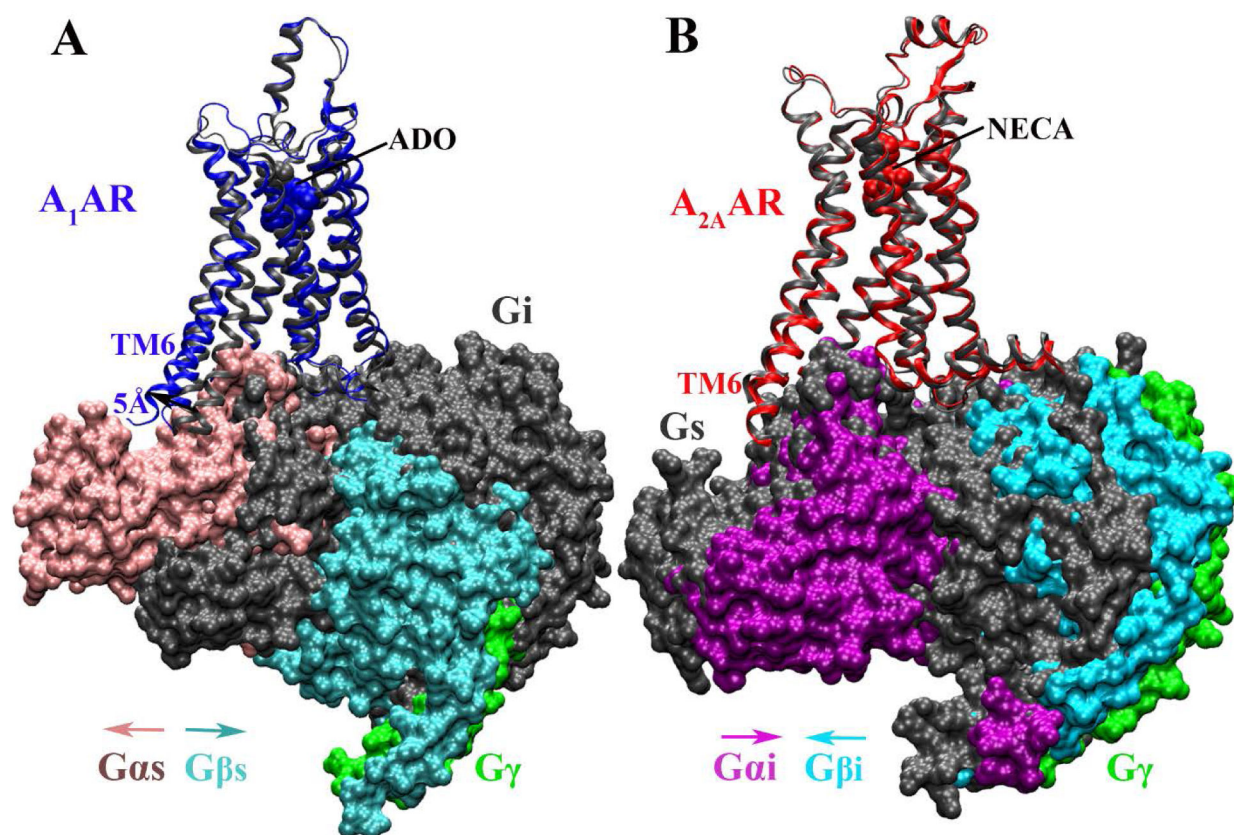
Figure 6.
Summary of specific AR-G protein interactions: (**A**) the ADO-bound A_1AR prefers to bind the G_i protein to the G_s. The latter could not stabilize agonist ADO binding in the A_1AR and tended to dissociate from the receptor. (**B**) The $A_{2A}AR$ could bind both the G_s and G_i proteins, which adopted distinct conformations in the complexes.

Table 1

Summary of GaMD simulations performed on the agonist-bound AR-G protein complexes.

System	A_1AR-G_i	$A_{2A}AR$-G_s	$A_{2A}AR$-G_i	A_1AR-G_s [e]
Dimension (Å^3)	112x124x150	110x124x148	110x124x148	108x124x153
N_{atoms}	180,394	175,140	176,028	176,940
Simulation Length (ns)	300 x 3	300 x 3	300 x 3	300 x 3
Boost Potential (kcal/mol)	21.43 ± 6.50	21.12 ± 6.49	20.96 ± 6.41	21.88 ± 6.58
Cryo-EM/Simulation starting structures				
AR:NPxxY-G:α5 Distance [a] (Å)	12.7	13.6	12.3	14.2
$Arg^{3.50}$- $Glu^{6.30}$ Distance [b] (Å)	16.3	18.4	18.4	16.3
α5 Orientation Angle [c] (°)	143.9	123.5	147.2	129.8
GaMD simulation low-energy conformations				
AR:NPxxY-G:α5 Distance (Å)	12.2	13.2	11.2	11.8, 13.5
$Arg^{3.50}$- $Glu^{6.30}$ Distance (Å)	17.4	18.2	17.6	17.5, 22.5
α5 Orientation Angle (°)	135.2	127.5	140.2	123.0, 130.0
Increase of G_α-G_β Distance [d] (Å)	−1.3	1.5	−0.8	1.2, 3.2

[a] The AR:NPxxY-G:α5 distance is the center-of-mass (COM) distance between the receptor NPxxY motif and the last 5 residues of the G_α α5 helix.

[b] The $Arg^{3.50}$-$Glu^{6.30}$ distance is the distance between the Cα atoms of conserved residues $Arg^{3.50}$ and $Glu^{6.30}$ in the receptors.

[c] The α5 orientation angle is the angle between COMs of the receptor orthosteric pocket, the last 5 and first 5 residues of the G_α α5 helix, illustrated in Figure S9E.

[d] The increase of G_α-G_β distance is the increase in the distance between COMs of the G_α (excluding the N-terminal helix) and G_β (excluding the C-terminal of β sheet) subunits compared to the cryo-EM structure.

[e] Two low energy conformations are identified from the GaMD simulations and thus two values are presented for simulations of the A_1AR-G_s complex.